



Metal-organic frameworks derived platinum-cobalt bimetallic nanoparticles in nitrogen-doped hollow porous carbon capsules as a highly active and durable catalyst for oxygen reduction reaction



Jie Ying^a, Jing Li^b, Gaopeng Jiang^a, Zachary Paul Cano^a, Zhong Ma^a, Cheng Zhong^c, Dong Su^b, Zhongwei Chen^{a,*}

^a Department of Chemical Engineering, University of Waterloo, Waterloo, Ontario, N2L 3G1, Canada

^b Center for Functional Nanomaterials, Brookhaven National Laboratory, Upton, NY, 11973, USA

^c Key Laboratory of Advanced Ceramics and Machining Technology (Ministry of Education), School of Materials Science and Engineering, Tianjin University, Tianjin, 300072, China

ARTICLE INFO

Keywords:

PtCo bimetallic nanoparticles
Metal-organic frameworks
Nitrogen-doping
Hollow porous capsules
Oxygen reduction reaction

ABSTRACT

Pt-based nanomaterials are regarded as the most efficient electrocatalysts for the oxygen reduction reaction (ORR) in proton exchange membrane fuel cells (PEMFCs). However, widespread adoption of PEMFCs requires solutions to major challenges encountered with ORR catalysts, namely high cost, sluggish kinetics, and low durability. Herein, a new efficient method utilizing Co-based metal-organic frameworks is developed to produce PtCo bimetallic nanoparticles embedded in unique nitrogen-doped hollow porous carbon capsules. The obtained catalyst demonstrates an outstanding ORR performance, with a mass activity that is 5.5 and 13.5 times greater than that of commercial Pt/C and Pt black, respectively. Most importantly, the product exhibits dramatically improved durability in terms of both electrochemically active surface area (ECAS) and mass activity compared to commercial Pt/C and Pt black catalysts. The remarkable ORR performance demonstrated here can be attributed to the structural features of the catalyst (its alloy structure, high dispersion and fine particle size) and the carbon support (its nitrogen dopant, large surface area and hollow porous structure).

1. Introduction

The proton exchange membrane fuel cell (PEMFC) has long been regarded as one of the most promising clean and efficient energy conversion devices for a wide variety of applications [1–3]. Its ability to provide on-demand power from hydrogen, which importantly can be stored on a seasonal basis, makes it a vital component of future zero-carbon energy grids [4,5]. However, the sluggish kinetics of the oxygen reduction reaction (ORR) at the cathode is currently preventing extensive usage of PEMFCs due to the consequential reduction in energy efficiency [6–8]. Existing carbon-supported Pt-based electrocatalysts can efficiently catalyze the ORR [9–13], but the scarcity and high cost of Pt as well as its poor stability still limit the practical applications of PEMFCs [1,2,14]. To tackle these challenges, the ORR catalyst community has traditionally focused on (i) engineering of the morphology, structure and component of Pt-based catalysts and (ii) optimization of the catalyst supports, for the purpose of maximizing both activity and durability.

Regarding the first strategy, an effective method of indirectly

reducing the Pt mass requirement is to improve the ORR activity and stability of Pt-based catalysts via advanced morphologies and structures [15–18]. Meanwhile, alloying of Pt with a secondary metal can further enhance the performance of Pt-based catalysts and concurrently reduce the usage of Pt [19,20]. These bimetallic nanostructured Pt-based materials can exhibit a superior activity and stability with an optimized oxygen absorption energy [21]. Among all Pt-based bimetallic nanomaterials, alloys of Pt and transition metals, in particular PtCo and PtNi, have been identified as the most active and stable catalysts for ORR by numerous studies [22–27]. The second strategy involves rational design the catalyst supports [28]. One effective method is to introduce heteroatom dopants such as nitrogen into the carbon support, which can not only increase chemical binding or “tethering” between the catalyst and support, but also largely facilitate interfacial electron transfer and adsorption of reactants (such as O₂) by modifying the charge of adjacent C atoms [29,30]. Moreover, supports with well-designed nanostructures such as carbon nanotubes [31,32], hollow carbon spheres [33,34], and hollow porous carbons (HPCs) [35–38] further improve the ORR activity and stability for Pt-based catalysts.

* Corresponding author.

E-mail address: zhwchen@uwaterloo.ca (Z. Chen).

Particularly, when HPCs encapsulate metal nanocrystals, the hybrid catalysts often exhibit remarkable catalytic activity and stability due to the high surface area, efficient mass transport, excellent conductivity and high electrochemical stability of HPCs along with the shell protection of the metal nanocrystals against aggregation/sintering [36–39].

Ideally, one should combine the above strategies such as high catalyst dispersion, transition metal alloying of Pt, heteroatom-doping of carbon support, and creation of a HPC structure to produce a top-performing Pt-based catalyst. More specifically, we envision that PtCo nanoparticles encapsulated in nitrogen-doped HPC would meet the exceptional ORR activity and durability requirements for commercial PEMFCs. However, it remains a great challenge to obtain this model catalyst owing to tedious and complex synthesis procedures currently described in the literature. Therefore, a procedure that can effectively and consistently produce the aforementioned hybrid material is highly desired.

In this study, we report for the first time an efficient method for synthesizing PtCo bimetallic nanoparticles mixed with Co nanoparticles encapsulated in nitrogen-doped hollow porous carbon capsules (denoted as PtCo/Co@NHPCC). It is derived from metal-organic frameworks (MOFs) via three steps, including introduction of Pt within the MOFs by a hydrophobic/hydrophilic approach, coating with a polymer shell, and finally a thermal treatment. The prepared products possess many desirable features such as well-dispersed nanoparticles, embedded alloys, hollow porous structures, capsule-like morphology, and nitrogen dopants. The obtained PtCo/Co@NHPCC displays an excellent catalytic activity for ORR in terms of mass activity and specific activity ($0.566 \text{ A mg}_{\text{Pt}}^{-1}$ and 0.876 mA cm^{-2}), which are much better than those of the commercial Pt/C catalysts ($0.102 \text{ A mg}_{\text{Pt}}^{-1}$ and 0.177 mA cm^{-2}) and commercial Pt black ($0.042 \text{ A mg}_{\text{Pt}}^{-1}$ and 0.221 mA cm^{-2}). More notably, PtCo/Co@NHPCC exhibits outstanding structural stability and catalytic durability, as it shows no obvious change in its nanostructure and only a slight ORR activity change after 5000 potential sweeps. This work demonstrates that PtCo/Co@NHPCC, which owns the advantages of both Pt alloys and advanced supports, are indeed a promising ORR electrocatalyst with improved activity, durability, and utilization efficiency of Pt.

2. Experimental section

2.1. Preparation of ZIF-67

ZIF-67 materials were synthesized according to the published literature with a slight modification [40]. In a typical synthesis of ZIF-67, 0.718 g of $\text{Co}(\text{NO}_3)_2 \cdot 6\text{H}_2\text{O}$ and 1.622 g of 2-methylimidazole were respectively dissolved in 50 mL of methanol at room temperature, and then mixed under vigorous stirring. After 20 min, the stirring was stopped and the mixture was kept in the static state for 20 h. The products were collected by centrifugation and washed with methanol several times, followed by vacuum drying at 80°C overnight.

2.2. Preparation of Pt@ZIF-67

In a typical synthesis of Pt@ZIF-67, 200 mg of dried ZIF-67 was dispersed in 30 mL of *n*-hexane and the mixture was sonicated for 30 min until it became homogeneous. After 2 h stirring, 0.4 mL of 30 mM aqueous $\text{H}_2\text{PtCl}_6 \cdot 6\text{H}_2\text{O}$ solution was added slowly and the solution was kept stirring for another 2 h. The products were collected by filtrating and drying at 150°C overnight, followed by treating in a gas flow of H_2/Ar (1/9) at 200°C for 5 h to yield Pt@ZIF-67.

2.3. Preparation of PtCo/Co@NHPCC

In a typical synthesis of PtCo/Co@NHPCC, 120 mg of Pt@ZIF-67 was dispersed in 10 mL of deionized water by sonicating. 3 mL of

24 mM tannic acid was adjusted to pH 8 by adding 6 M KOH aqueous solution. Then, the Pt@ZIF-67 solution was poured into the tannic acid solution under stirring. After 6 min, Pt@ZIF-67@TA was collected by centrifugation, washed with methanol three times, and dried under vacuum overnight. Finally, PtCo/Co@NHPCC was obtained by calcining Pt@ZIF-67@TA under an argon flow at 800°C for 2 h.

2.4. Characterization

X-ray diffraction (XRD) patterns were collected on a XRD 3000 diffractometer equipped with Cu K_α radiation. Scanning electron microscopy (SEM) experiments were carried out on a LEO FESEM 1530 and S-4800 electron microscope. Transmission electron microscopy (TEM) images were collected on a JEOL 2010F microscope. The nitrogen adsorption and desorption isotherms were measured by using a Micromeritics ASAP 3020 system. Before the adsorption/desorption measurements, the samples were outgassed for 8 h at 180°C . The BET specific surface area was evaluated from adsorption data in the relative pressure range of 0.1–0.3. The amount of catalysts was determined by the inductively coupled plasma atomic emission spectroscopy (Perkin Elmer Ltd., USA).

2.5. Electrochemical measurements

A three-electrode cell was used for electrochemical measurements. A platinum wire was used as a counter electrode and a reversible hydrogen electrode (RHE) was used as a reference electrode. The working electrode was a glassy-carbon Rotating Disk Electrode (RDE, diameter: 5 mm, area: 0.196 cm^2). The Pt loading on glassy-carbon was $6.5 \mu\text{g cm}^{-2}$ for PtCo/Co@NHPCC. Cyclic voltammetry (CV) curves were collected in 0.1 M HClO_4 solutions under a flow of N_2 at a sweep rate of 50 mV s^{-1} . ORR measurements were carried out in 0.1 M HClO_4 solutions under the flow of O_2 using a glassy-carbon RDE at a rotation rate of 1600 rpm with a sweep rate of 10 mV s^{-1} . The electrochemically active surface area (ECSA) measurements were determined by integrating the hydrogen adsorption/desorption charge on the CV. The accelerated durability tests (ADTs) were performed at room temperature in O_2 -saturated 0.1 M HClO_4 solution by applying cyclic potential sweeps between 0.6 and 1.1 V versus RHE at a sweep rate of 50 mV s^{-1} for 5000 cycles. For comparison, commercial Pt/C catalyst (TKK, 28.2 wt% Pt) and Pt black (Sigma-Aldrich, 99.9% fuel cell grade) were used as the benchmarks, and the same procedure as described above was used to conduct the electrochemical measurement, except that the Pt loadings were $20.0 \mu\text{g cm}^{-2}$ for Pt/C and $51.0 \mu\text{g cm}^{-2}$ for Pt black catalysts.

3. Results and discussion

The overall synthesis procedure of the hybrid catalyst PtCo/Co@NHPCC is illustrated in Fig. 1. Pt nanoparticles are firstly encapsulated and dispersed into MOFs via the following hydrophobic/hydrophilic method: (i) synthesis of ZIF-67 [40,41], a Co-based highly porous MOF with high nitrogen content and a hydrophilic nature, as the starting materials (Fig. 1a); (ii) dispersion of ZIF-67 in *n*-hexane, a hydrophobic solvent that cannot enter into the pores of ZIF-67 due to the high hydrophilicity of ZIF-67 (Fig. 1b); (iii) absorption of Pt precursor into the pores of ZIF-67 due to its hydrophilic affinity to ZIF-67 (Fig. 1c); (iv) removal of all of the solvents via evaporation (Fig. 1d) and (v) formation of Pt nanoparticles in the pores of ZIF-67 (Pt@ZIF-67) by hydrogen reduction (Fig. 1e). The amounts of both solvents play important roles; a small amount (no more than the pore volume of ZIF-67 used) of metal precursor aqueous solution can be totally absorbed into the pores of ZIF-67 through capillary forces, while the large amount of *n*-hexane can help disperse ZIF-67. The latter solvent creates the repulsive outer hydrophobic environment around ZIF-67 and facilitates the absorption process. After completion of the above method, the as-synthesized Pt@

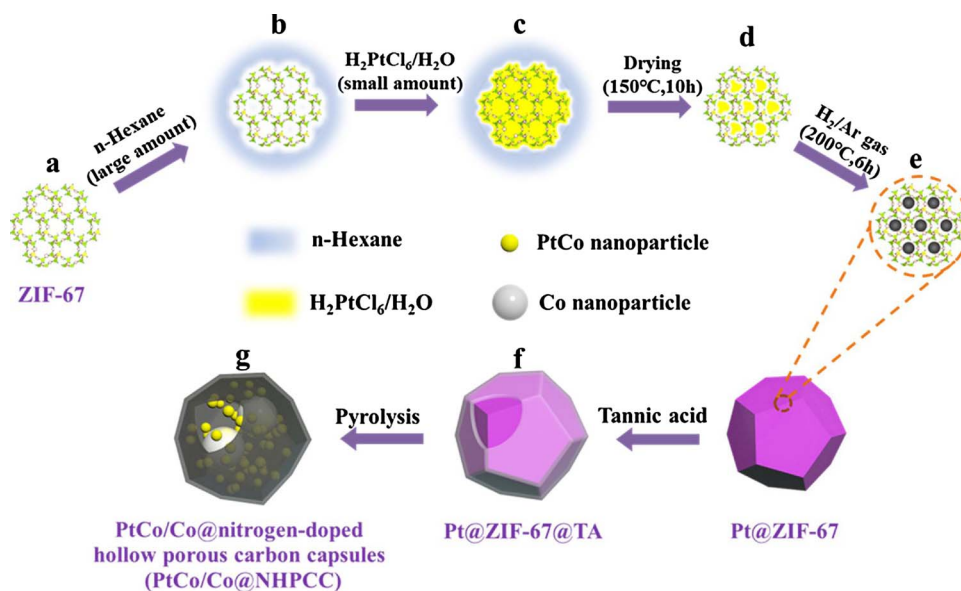


Fig. 1. Schematic representation of the preparation of PtCo/Co@NHPCC.

ZIF-67 is covered with a polymer coating of tannic acid, yielding a product denoted as Pt@ZIF-67@TA (Fig. 1f). Finally, pyrolysis of Pt@ZIF-67@TA at high temperature is carried out under the protection of an inert atmosphere; this step triggers three separate phenomena which combine to create the elusive combination of a finely dispersed PtCo structure and a protective and catalytically active nitrogen-doped porous carbon capsule. Firstly, the tannic acid coating forms the hollow and porous carbon capsule which maintains the conformal morphology templated from polyhedral ZIF-67 through the pyrolysis treatment. Secondly, diffusion of the Co from ZIF-67 and the Pt nanoparticles during pyrolysis produces a unique combination of very small PtCo bimetallic nanoparticles and relatively large Co monometallic nanoparticles. Thirdly, diffusion of nitrogen from the ZIF-67 structure efficiently introduces the nitrogen dopant into the porous carbon capsule, therefore resulting in the final PtCo/Co@NHPCC product (Fig. 1g).

SEM images for ZIF-67, Pt@ZIF-67, Pt@ZIF-67@TA, and PtCo/Co@NHPCC are shown in Fig. 2a–d. ZIF-67 synthesized via a simple method in methanol solution at room temperature exhibits a polyhedral shape with an average particle size of ~300 nm (Fig. 2a). The XRD (Fig. S1a) and N₂ adsorption-desorption (Fig. S2a) results confirm the highly crystalline structure and high porosity of ZIF-67, which are in good agreement with the previous literature [40]. After encapsulating Pt nanoparticles in the pores of ZIF-67 through the hydrophobic/hydrophilic method, the obtained Pt@ZIF-67 displayed a similar surface morphology to pristine ZIF-67 (Fig. 2b), and Pt nanoparticles were well-dispersed within ZIF-67 (Fig. S3). The non-visualized color change after Pt encapsulation (Fig. S4) also suggests the homogeneous dispersion of Pt nanoparticles in the ZIF-67. Pt@ZIF-67 shows similar diffraction peak positions and intensities to those of ZIF-67 (Fig. S1b), indicating that the framework of ZIF-67 remains intact after encapsulation of Pt. No characteristic peaks for Pt appeared in the XRD pattern of Pt@ZIF-67, demonstrating the formation of ultrafine Pt nanoparticles. From the N₂ absorption-desorption data (Fig. S2b and Table S1), compared with pristine ZIF-67, both the Brunauer-Emmett-Teller (BET) surface area and pore volume of Pt@ZIF-67 have largely decreased, suggesting the successful immobilization of Pt nanoparticles inside the pores of ZIF-67. Fig. 2c and Fig. S5 show the SEM images of Pt@ZIF-67@TA. It is clearly revealed that the core-shell nanostructures of Pt@ZIF-67@TA include a thin and conformal shell layer of TA over the polyhedral shape of the core Pt@ZIF-67.

PtCo/Co@NHPCC shown in Fig. 2d exhibits a uniform capsule-like morphology and conformal shape, indicating the retention of the polyhedral shape of Pt@ZIF-67@TA during carbonization by pyrolysis

treatment. The TEM images (Fig. 2e,f) of PtCo/Co@NHPCC exhibit a novel hollow porous structure, where the outer shell layer was derived from carbonization of polymer TA and the inner porous nanostructure was evolved from ZIF-67 by the high-temperature process. The hollow structure with interior porous features is presented more clearly in the high-angle annular dark-field scanning TEM (HAADF-STEM) image (Fig. 2g). Moreover, N₂ adsorption-desorption measurement further confirms the highly porous nature of PtCo/Co@NHPCC, which shows a high BET surface area of 356 m² g⁻¹ (Fig. S2c and Table S1). As shown in the TEM and STEM images (Fig. 2f,g) of PtCo/Co@NHPCC, many nanoparticles with various sizes in the range of one to dozens of nanometers are highly dispersed inside the hollow porous capsules. To verify the composition of these nanoparticles in PtCo/Co@NHPCC, the element mapping and XRD were performed. As shown in Fig. 2j,k, Pt elements are well-dispersed, thus corresponding to the relatively small nanoparticles, while Co elements are mainly concentrated in the relatively large nanoparticles, indicating the different compositions of these nanoparticles. The XRD pattern of PtCo/Co@NHPCC (Fig. 2l and Fig. S1d) shows four intense peaks at the values of 41.6°, 44.2°, 51.5° and 75.9°. The peaks at 44.2°, 51.5° and 75.9° can be assigned to the typical (111), (200), and (220) planes of the face-centered cubic (fcc) structure of Co (JCPDS no. 15-0806). Another peak of 41.6° located between the peak positions of the Pt (111) plane (JCPDS no. 04-0802) and Co (111) plane can be reasonably ascribed to the (111) plane of PtCo alloy, which is caused by the change of the lattice parameters via the incorporation of Co in the fcc structure of Pt during the formation of the alloyed structure [37]. The broad peak of the PtCo (111) plane also indicates the small particle sizes. Therefore, these nanoparticles are inferred to be a combination of small PtCo bimetallic nanocrystals and large Co monometallic nanocrystals. To definitively prove the nature of the nanoparticles, PtCo/Co@NHPCC was further measured by SAED (selected area electron diffraction), FFT (fast Fourier transform), and EDX (energy-dispersive X-ray spectroscopy) analysis (Fig. 3). As shown in Fig. 3a and its inset, the SAED pattern acquired on a large area including large and small particles displays sets of both sharp diffraction spots and concentric rings, which can be indexed with fcc Co and PtCo, respectively. This is in good agreement with the XRD results. For a large particle (Fig. 3b), the FFT pattern shows the diffraction spots of Co (inset of Fig. 3b), while PtCo diffraction spots are displayed in the FFT pattern from a small particle (Fig. 3c and inset). Furthermore, the EDX analysis of 10 large particles and 10 small particles further demonstrates that the nanoparticles in PtCo/Co@NHPCC consist of large Co nanocrystals and small PtCo bimetallic nanocrystals (Fig. 3d–f).

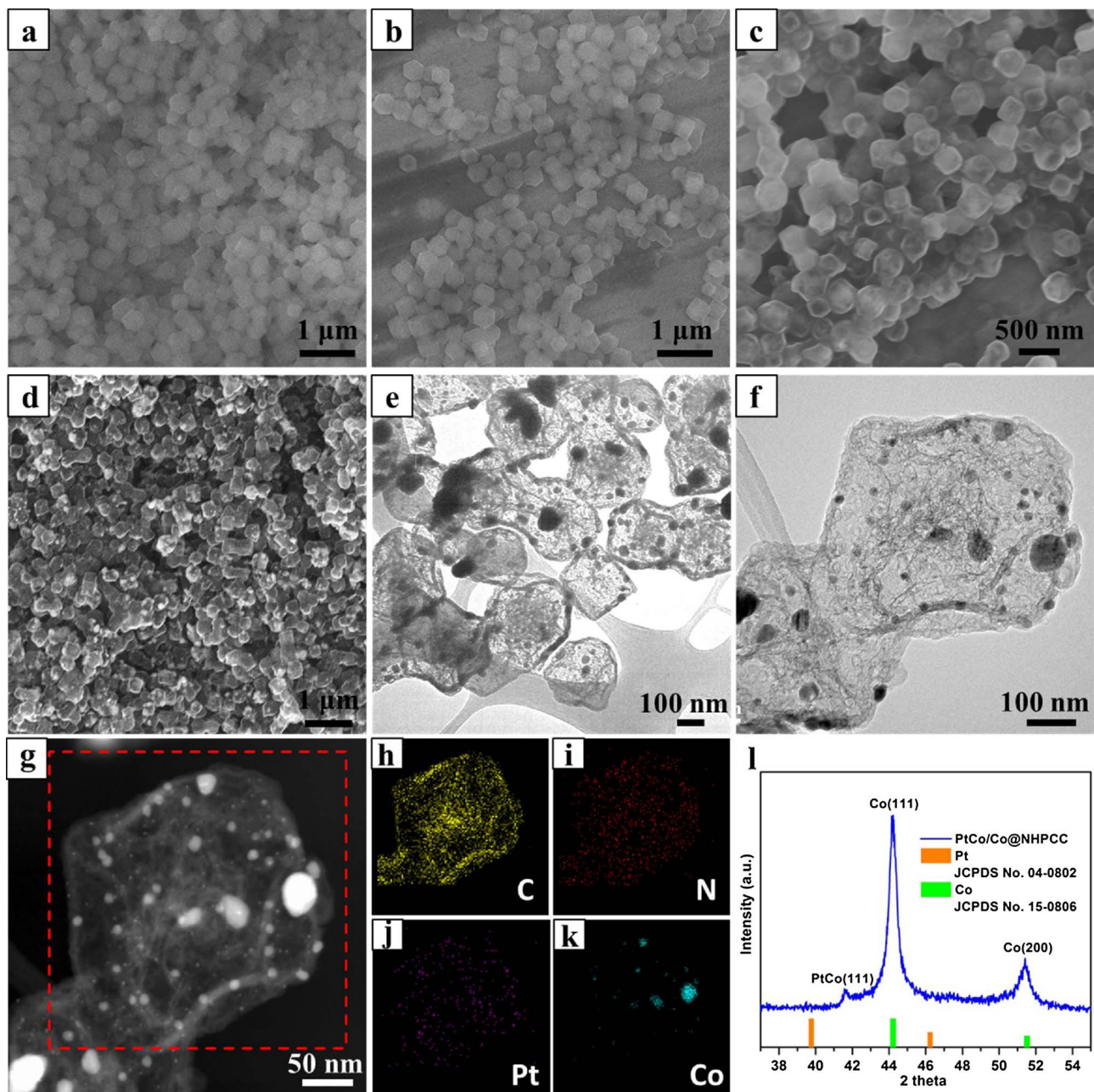


Fig. 2. SEM images of (a) ZIF-67, (b) Pt@ZIF-67, (c) Pt@ZIF-67@TA, and (d) PtCo/Co@NHPCC. (e) TEM, (f) HRTEM, and (g) HAADF-STEM images of PtCo/Co@NHPCC. (h-k) Elemental mapping results of PtCo/Co@NHPCC: h) C (yellow), i) N (red), j) Pt (purple), and k) Co (blue). (l) XRD pattern of PtCo/Co@NHPCC. (For interpretation of the references to colour in this figure legend, the reader is referred to the web version of this article.)

Element mappings of carbon and nitrogen shown in Fig. 2h,i display that the carbon and nitrogen elements are homogeneously distributed throughout the hollow porous capsule, demonstrating their nitrogen-doped carbon feature. The X-ray photoelectron spectroscopy (XPS) study (Fig. S6) of PtCo/Co@NHPCC at the N 1 s levels further confirms the nitrogen-doped character. Additionally, the nitrogen species in PtCo/Co@NHPCC are mainly pyridinic N and graphitic N, which have been demonstrated to improve the ORR activity and enhance the adhesion between Pt catalysts and supports, resulting in improved stability [42,43]. Thus, all the results fully confirm the successful formation of small PtCo bimetallic nanoparticles encapsulated in unique nitrogen-doped hollow porous carbon capsules.

In virtue of their unique hollow porous nanostructures with the beneficial features of embedded small alloyed particles, nitrogen-doped carbon, and high surface area, PtCo/Co@NHPCC is expected to exhibit

significantly superior catalytic performance to traditional Pt-based catalysts, particularly in electrocatalysis. Thus, the electrocatalytic property of PtCo/Co@NHPCC was evaluated toward the ORR. For comparison to baseline performance, commercial Pt/C (Fig. S7a) and Pt black (Fig. S7c) catalysts were also investigated under the same condition. Fig. 4a shows the CV curves of the three catalysts performed at room temperature in N₂-purged 0.1 M HClO₄ solution with a sweep rate of 50 mV s⁻¹. The ECSA was calculated by integrating the charge collected in the hydrogen adsorption/desorption region from the electrode surface after double-layer correction and assuming a value of 210 μ C cm⁻² for the adsorption of a hydrogen monolayer. PtCo/Co@NHPCC exhibits a considerably high ECSA of 64.6 m² g⁻¹ based on the Pt mass, which is even slightly higher than that of commercial Pt/C (57.6 m² g⁻¹), and much higher than that of Pt black (19.0 m² g⁻¹). To some extent, the high ECSA also can confirm the small particle size of

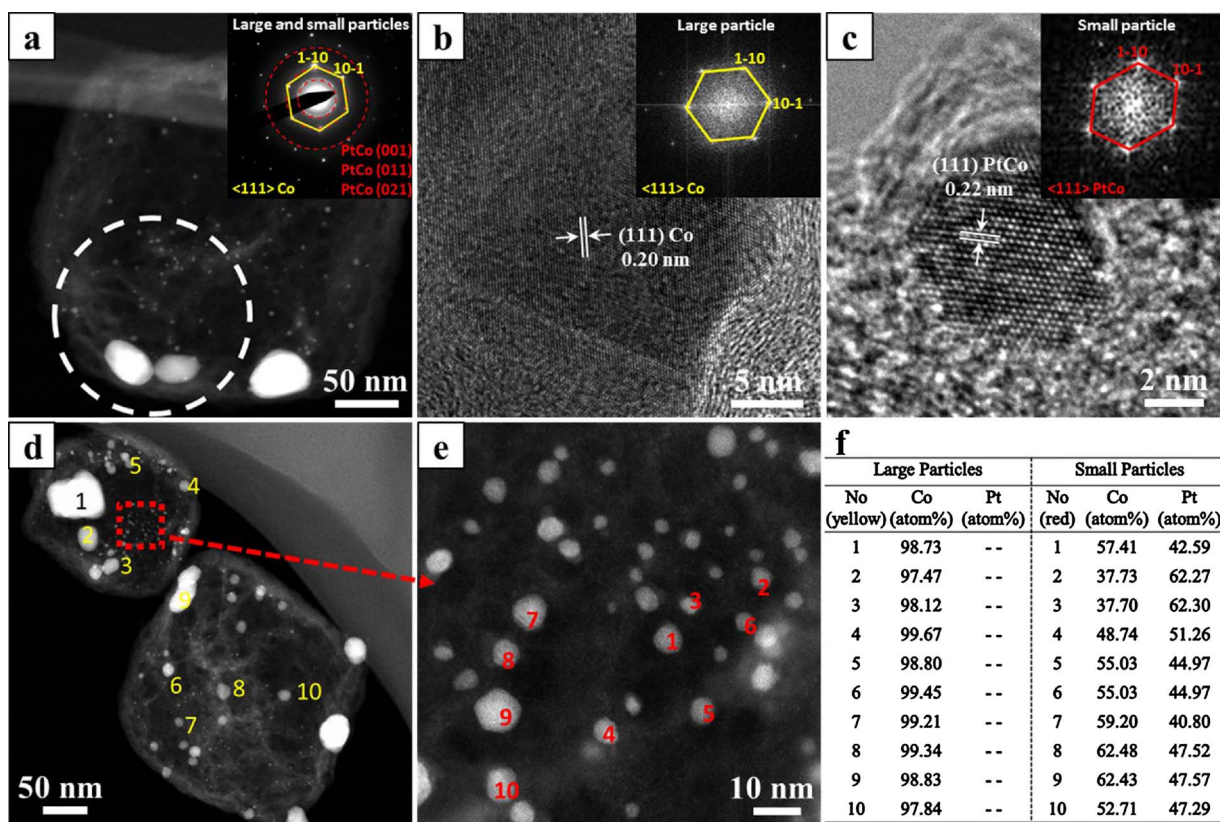


Fig. 3. (a) HAADF-STEM image of PtCo/Co@NHPCC. Inset is SAED pattern recorded from a). (b) HRTEM image of a large particle from PtCo/Co@NHPCC and corresponding FFT image (inset). (c) HRTEM image of a small particle from PtCo/Co@NHPCC and corresponding FFT image (inset). (d,e) HAADF-STEM images of PtCo/Co@NHPCC and (f) corresponding EDX analysis for individual nanoparticles as labelled by numbers.

PtCo alloys in PtCo/Co@NHPCC, which is consistent with the SAED, FFT, and EDX data. The ORR tests were performed in O₂-saturated 0.1 M HClO₄ solutions by using a glassy carbon rotating disk electrode (RDE) at room temperature with a sweep rate of 10 mV s⁻¹. Fig. 4b shows the ORR polarization curves for PtCo/Co@NHPCC, commercial

Pt/C, and Pt black. The half-wave potential of PtCo/Co@NHPCC is 0.883 V, which is higher than that of commercial Pt/C (0.864 V) and Pt black (0.868 V), indicating the best activity of PtCo/Co@NHPCC among these three catalysts. In addition, the Tafel slopes of these catalysts at low over-potentials are close to 60 mV/decade (Fig. S8), indicating that

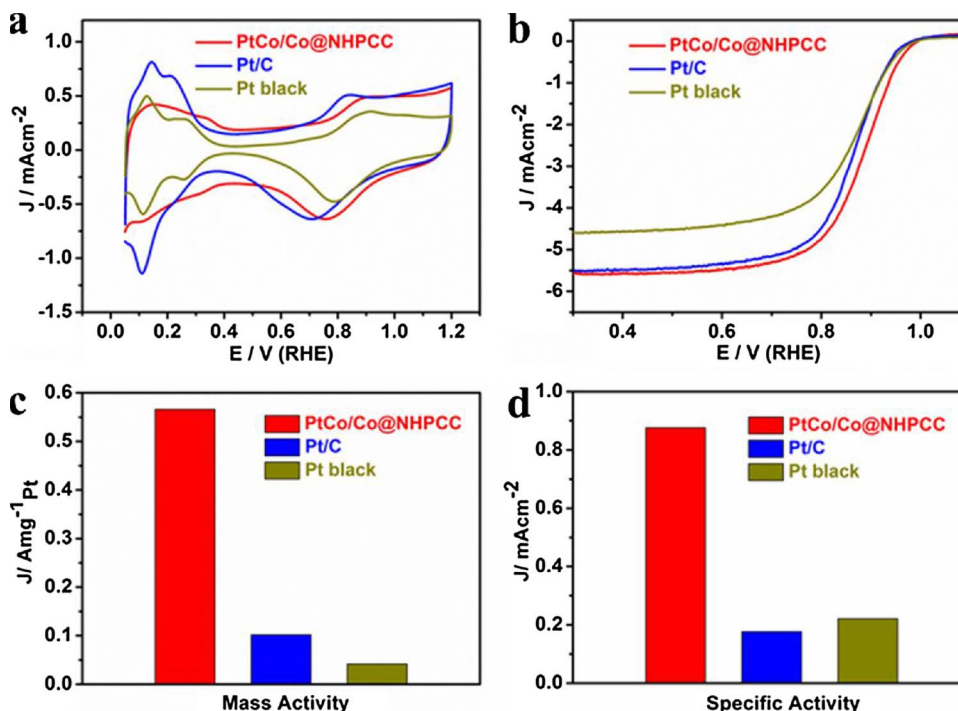


Fig. 4. (a) CV curves, (b) ORR polarization curves, (c) mass activity, and (d) specific activity at 0.9 V versus RHE for PtCo/Co@NHPCC, Pt/C, and Pt black catalysts.

their rate determining steps are pseudo two electron procedures [44,45]. According to the Koutecky-Levich equation [46,47], the kinetic current density, which represents the intrinsic activity of the electrocatalyst, was calculated and then normalized with respect to the mass loading of Pt and ECSA to obtain the mass activity and specific activity, respectively (Table S2). As shown in Fig. 4c, PtCo/Co@NHPCC demonstrates an outstanding mass activity of $0.566 \text{ A mg}_{\text{Pt}}^{-1}$, which is 5.5 and 13.5 times greater than that of commercial Pt/C ($0.102 \text{ A mg}_{\text{Pt}}^{-1}$) and Pt black ($0.042 \text{ A mg}_{\text{Pt}}^{-1}$), respectively. Likewise, as observed in Fig. 4d, the specific activity of PtCo/Co@NHPCC (0.876 mA cm^{-2}) is 4.9 and 4.0 times greater than that of commercial Pt/C (0.177 mA cm^{-2}) and Pt black (0.221 mA cm^{-2}), respectively. Notably, both the mass activity and specific activity of PtCo/Co@NHPCC ($0.566 \text{ A mg}_{\text{Pt}}^{-1}$ and 0.876 mA cm^{-2}) are superior to that of the previously reported PtCo/C catalysts (Table S3) and the U.S. Department of Energy (DOE) 2017 targets of $0.440 \text{ A mg}_{\text{Pt}}^{-1}$ and 0.720 mA cm^{-2} , respectively [2].

The ADTs of PtCo/Co@NHPCC, commercial Pt/C, and Pt black were also conducted to assess the ORR stability of the catalyst by performing 5000 potential cycles sweeping between 0.6 and 1.1 V versus a RHE at the rate of 50 mV s^{-1} in O_2 -saturated 0.1 M HClO_4 solution at room temperature. Fig. 5a-c show the CV curves of these three catalysts before and after ADT. In comparison with the dramatic drops in the current densities of the peaks in the hydrogen adsorption/desorption regions for commercial Pt/C and Pt black after ADT, the drop for PtCo/Co@NHPCC is only marginal. As shown in Fig. 5g, PtCo/Co@NHPCC shows a loss of 29.8% in ECSA after ADT, whereas commercial Pt/C and Pt black display losses of 53.2% and 41.4% in ECSA, indicating that the durability of PtCo/Co@NHPCC is much better than commercial Pt/C and Pt black. Fig. 5d-f plot the polarization curves of these three catalysts before and after ADT. Only a 19 mV loss in half-wave potential

for PtCo/Co@NHPCC is observed after ADT, which is much lower in comparison with 67 mV and 74 mV half-wave potential losses for commercial Pt/C and Pt black, respectively. The mass activities of these three catalysts on the basis of Pt mass before and after ADT are given in Fig. 5h. Notably, PtCo/Co@NHPCC retains 62.7% of the initial mass activity with a high value of $0.355 \text{ A mg}_{\text{Pt}}^{-1}$ after ADT, which is still 3.5 and 8.5 times greater than that of pristine commercial Pt/C and Pt black, respectively. As comparisons, the retentions in mass activities for commercial Pt/C and Pt black are 16.7% and 20.5%, respectively. Similarly, 89.4% of the initial specific activity is observed for PtCo/Co@NHPCC after ADT, while 35.6% and 35.3% are retained for commercial Pt/C and Pt black, respectively (Fig. 5i). These results definitively demonstrate that PtCo/Co@NHPCC has an excellent ORR durability which is far better than that of commercial Pt/C and Pt black. To clarify the reasons of their different durability, the morphologies of these three catalysts after ADT were investigated by TEM. As shown in Fig. S7e,f, the morphology and hollow porous structure of PtCo/Co@NHPCC shows no obvious change, except for the elimination of the large Co particles in the capsules due to the dissolution of the unstable Co metals in acid solution during ADT [48,49]. By contrast, severe aggregation/sintering after ADT (Fig. S7b,d) are observed for both commercial Pt/C and black Pt, resulting in their poor durability. Overall, PtCo/Co@NHPCC has demonstrated an outstanding ORR activity, stability, and durability, which should be attributed to its unique features: i) alloy structure and fine size of PtCo nanoparticles which improves the intrinsic activity, stability, and utilization efficiency of Pt; ii) nitrogen-doping and high surface area of hollow porous carbon capsules that facilitate the electron transport and oxygen diffusion in the ORR; iii) synergistic effect between bimetallic catalyst and novel nanostructured carbon support, which further enhances their activity and durability.

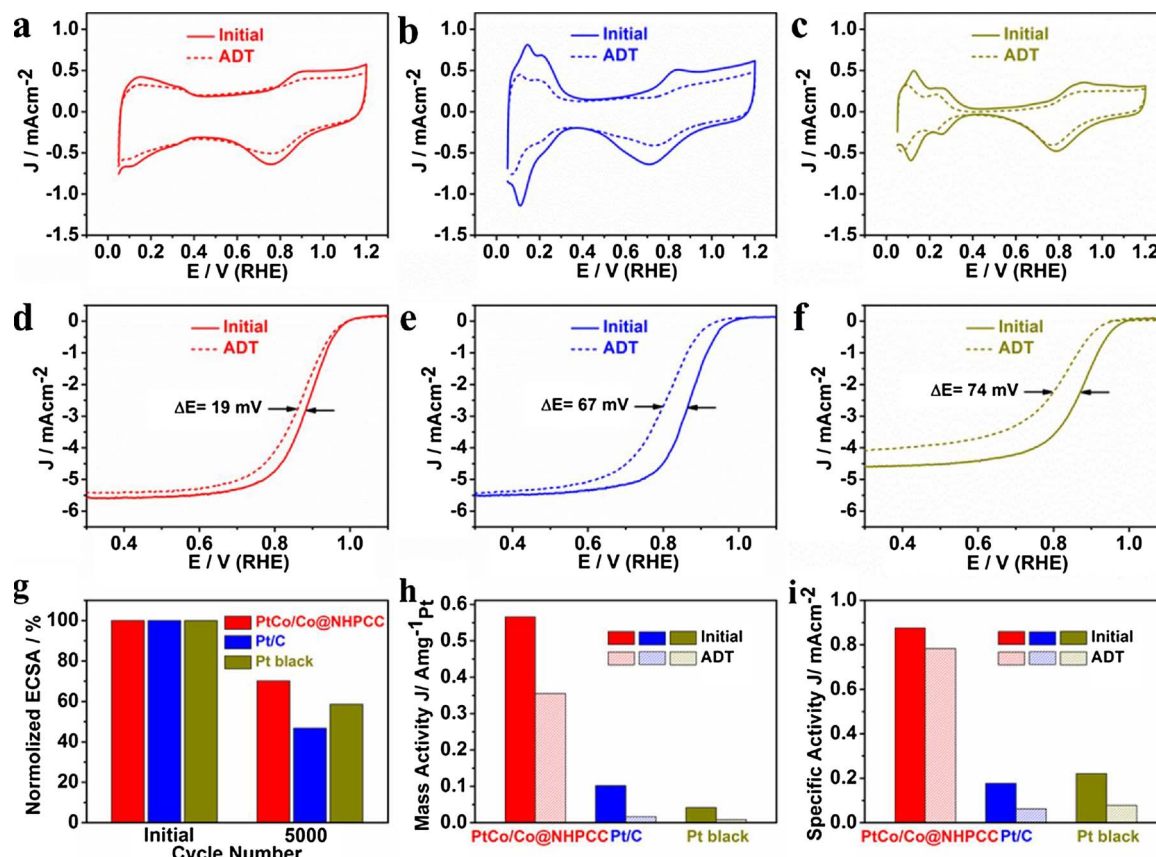


Fig. 5. CV curves of (a) PtCo/Co@NHPCC, (b) Pt/C, and (c) Pt black, ORR polarization curves of (d) PtCo/Co@NHPCC, (e) Pt/C, and (f) Pt black before and after ADT, and corresponding summary of (g) ECSA, (h) mass activity, and (i) specific activity for PtCo/Co@NHPCC, Pt/C, and Pt black before and after ADT, respectively.

4. Conclusions

In summary, we have presented an efficient and novel strategy to rationally design and synthesize PtCo bimetallic nanoparticles embedded in unique nitrogen-doped hollow porous carbon capsules. PtCo/Co@NHPCC shows much superior ORR activity and durability in comparison to commercial Pt/C and Pt black. Notably, both the mass activity (0.566 A mg_{Pt}⁻¹) and specific activity (0.876 mA cm⁻²) of PtCo/Co@NHPCC are beyond the U.S. DOE recommended 2017 target of 0.440 A mg_{Pt}⁻¹ and 0.720 mA cm⁻², respectively. The excellent ORR performance of PtCo/Co@NHPCC could be ascribed to the multitude of features of the catalyst and support, including the alloy structure, small particle size, high dispersion, nitrogen-dopant, high surface area, and hollow porous structure. Our investigation shows that advanced ORR electrocatalysts can be developed by combining the advantages of superior Pt-based nanostructured catalysts and novel support materials, which ultimately supports the widespread commercial penetration of PEMFCs.

Acknowledgments

This work was supported by the Natural Sciences and Engineering Research Council of Canada (NSERC), the University of Waterloo, and the Waterloo Institute for Nanotechnology. The authors greatly acknowledge the Catalysis Research for Polymer Electrolyte Fuel Cells (CaRPE FC) Network administered from Simon Fraser Grant No. APCPJ 417858-11 through NSERC. TEM imaging was performed at the Canadian Center for Electron Microscopy (CCEM) located at McMaster University. Part of EM work was performed at the Center for Functional Nanomaterials, Brookhaven National Laboratory, which is supported by the U.S. Department of Energy (DOE), Office of Basic Energy Science, under Contract No. DE-SC0012704.

Appendix A. Supplementary data

Supplementary data associated with this article can be found, in the online version, at <https://doi.org/10.1016/j.apcatb.2017.11.077>.

References

- [1] M. Shao, Q. Chang, J.-P. Dodelet, R. Chenitz, Recent advances in electrocatalysts for oxygen reduction reaction, *Chem. Rev.* 116 (2016) 3594–3657.
- [2] E. Antolini, Structural parameters of supported fuel cell catalysts: the effect of particle size inter-particle distance and metal loading on catalytic activity and fuel cell performance, *Appl. Catal. B-Environ.* 181 (2016) 298–313.
- [3] Z. Chen, D. Higgins, A. Yu, L. Zhang, J. Zhang, A review on non-precious metal electrocatalysts for PEM fuel cells, *Energy Environ. Sci.* 4 (2011) 3167–3192.
- [4] M.A. Pellow, C.J. Emmott, C.J. Barnhart, S.M. Benson, Hydrogen or batteries for grid storage? a net energy analysis, *Energy Environ. Sci.* 8 (2015) 1938–1952.
- [5] G. Gahleitner, Hydrogen from renewable electricity: an international review of power-to-gas pilot plants for stationary applications, *Int. J. Hydrogen Energy* 38 (2013) 2039–2061.
- [6] Y. Nie, L. Li, Z. Wei, Recent advancements in Pt and Pt-free catalysts for oxygen reduction reaction, *Chem. Soc. Rev.* 44 (2015) 2168–2201.
- [7] X. Huang, Z. Zhao, L. Cao, Y. Chen, E. Zhu, Z. Lin, M. Li, A. Yan, A. Zettl, Y.M. Wang, High-performance transition metal-doped Pt₃Ni octahedra for oxygen reduction reaction, *Science* 348 (2015) 1230–1234.
- [8] Y. Lu, S. Du, R. Steinberger-Wilckens, One-dimensional nanostructured electrocatalysts for polymer electrolyte membrane fuel cells-A review, *Appl. Catal. B-Environ.* 199 (2016) 292–314.
- [9] J. Wu, H. Yang, Platinum-based oxygen reduction electrocatalysts, *Acc. Chem. Res.* 46 (2013) 1848–1857.
- [10] M. Li, Z. Zhao, T. Cheng, A. Fortunelli, C.-Y. Chen, R. Yu, Q. Zhang, L. Gu, B.V. Merinov, Z. Lin, Ultrafine jagged platinum nanowires enable ultrahigh mass activity for the oxygen reduction reaction, *Science* 354 (2016) 1414–1419.
- [11] J. Ying, X.-Y. Yang, Z.-Y. Hu, S.-C. Mu, C. Janiak, W. Geng, M. Pan, X. Ke, G. Van Tendeloo, B.-L. Su, One particle@one cell: highly monodispersed PtPd bimetallic nanoparticles for enhanced oxygen reduction reaction, *Nano Energy* 8 (2014) 214–222.
- [12] D. Higgins, M.A. Hoque, M.H. Seo, R. Wang, F. Hassan, J.Y. Choi, M. Pritzker, A. Yu, J. Zhang, Z. Chen, Development and simulation of sulfur-doped graphene supported platinum with exemplary stability and activity towards oxygen reduction, *Adv. Funct. Mater.* 24 (2014) 4325–4336.
- [13] M.A. Hoque, F.M. Hassan, M.-H. Seo, J.-Y. Choi, M. Pritzker, S. Knights, S. Ye, Z. Chen, Optimization of sulfur-doped graphene as an emerging platinum nanowires support for oxygen reduction reaction, *Nano Energy* 19 (2016) 27–38.
- [14] M.K. Debe, Electrocatalyst approaches and challenges for automotive fuel cells, *Nature* 486 (2012) 43–51.
- [15] L. Bu, N. Zhang, S. Guo, X. Zhang, J. Li, J. Yao, T. Wu, G. Lu, J.-Y. Ma, D. Su, Biaxially strained PtPb/Pt core/shell nanoplate boosts oxygen reduction catalysis, *Science* 354 (2016) 1410–1414.
- [16] C. Chen, Y. Kang, Z. Huo, Z. Zhu, W. Huang, H.L. Xin, J.D. Snyder, D. Li, J.A. Herron, M. Mavrikakis, Highly crystalline multimetallic nanoframes with three-dimensional electrocatalytic surfaces, *Science* 343 (2014) 1339–1343.
- [17] M.A. Hoque, F.M. Hassan, D. Higgins, J.Y. Choi, M. Pritzker, S. Knights, S. Ye, Z. Chen, Multigrain platinum nanowires consisting of oriented nanoparticles anchored on sulfur-doped graphene as a highly active and durable oxygen reduction electrocatalyst, *Adv. Mater.* 27 (2015) 1229–1234.
- [18] J. Ying, Z.-Y. Hu, X.-Y. Yang, H. Wei, Y.-X. Xiao, C. Janiak, S.-C. Mu, G. Tian, M. Pan, G. Van Tendeloo, High viscosity to highly dispersed PtPd bimetallic nanocrystals for enhanced catalytic activity and stability, *Chem. Commun.* 52 (2016) 8219–8222.
- [19] N.S. Porter, H. Wu, Z. Quan, J. Fang, Shape-control and electrocatalytic activity-enhancement of Pt-based bimetallic nanocrystals, *Acc. Chem. Res.* 46 (2013) 1867–1877.
- [20] J. Ying, X.-Y. Yang, G. Tian, C. Janiak, B.-L. Su, Self-assembly: an option to nanoporous metal nanocrystals, *Nanoscale* 6 (2014) 13370–13382.
- [21] J. Greeley, I. Stephen, A. Bondarenko, T.P. Johansson, H.A. Hansen, T. Jaramillo, J. Rossmeisl, I. Chorkendorff, J.K. Nørskov, Alloys of platinum and early transition metals as oxygen reduction electrocatalysts, *Nat. Chem.* 1 (2009) 552–556.
- [22] D. Wang, H.L. Xin, R. Hovden, H. Wang, Y. Yu, D.A. Muller, F.J. DiSalvo, H.D. Abruna, Structurally ordered intermetallic platinum-cobalt core-shell nanoparticles with enhanced activity and stability as oxygen reduction electrocatalysts, *Nat. Mater.* 12 (2013) 81–87.
- [23] L. Bu, S. Guo, X. Zhang, X. Shen, D. Su, G. Lu, X. Zhu, J. Yao, J. Guo, X. Huang, Surface engineering of hierarchical platinum-cobalt nanowires for efficient electrocatalysis, *Nat. Commun.* 7 (2016) 11850.
- [24] D.S. Choi, A.W. Robertson, J.H. Warner, S.O. Kim, H.H. Kim, Low-temperature chemical vapor deposition synthesis of Pt-Co alloyed nanoparticles with enhanced oxygen reduction reaction catalysis, *Adv. Mater.* 28 (2016) 7115–7122.
- [25] X. Huang, E. Zhu, Y. Chen, Y. Li, C.Y. Chiu, Y. Xu, Z. Lin, X. Duan, Y. Huang, A facile strategy to Pt₃Ni nanocrystals with highly porous features as an enhanced oxygen reduction reaction catalyst, *Adv. Mater.* 25 (2013) 2974–2979.
- [26] Z. Niu, N. Becknell, Y. Yu, D. Kim, C. Chen, N. Kornienko, G.A. Somorjai, P. Yang, Anisotropic phase segregation and migration of Pt in nanocrystals en route to nanoframe catalysts, *Nat. Mater.* 15 (2016) 1188–1194.
- [27] C. Cui, L. Gan, M. Hegggen, S. Rudi, P. Strasser, Compositional segregation in shaped Pt alloy nanoparticles and their structural behaviour during electrocatalysis, *Nat. Mater.* 12 (2013) 765–771.
- [28] Y.-J. Wang, N. Zhao, B. Fang, H. Li, X.T. Bi, H. Wang, Carbon-supported Pt-based alloy electrocatalysts for the oxygen reduction reaction in polymer electrolyte membrane fuel cells: particle size, shape, and composition manipulation and their impact to activity, *Chem. Rev.* 115 (2015) 3433–3467.
- [29] Z. Yang, H. Nie, X. Chen, X. Chen, S. Huang, Recent progress in doped carbon nanomaterials as effective cathode catalysts for fuel cell oxygen reduction reaction, *J. Power Sources* 236 (2013) 238–249.
- [30] Y. Zhou, K. Neyerlin, T.S. Olson, S. Pylypenko, J. Bult, H.N. Dinh, T. Gennett, Z. Shao, R. O’Hayre, Enhancement of Pt and Pt-alloy fuel cell catalyst activity and durability via nitrogen-modified carbon supports, *Energy Environ. Sci.* 3 (2010) 1437–1446.
- [31] Z. Liu, Q. Shi, R. Zhang, Q. Wang, G. Kang, F. Peng, Phosphorus-doped carbon nanotubes supported low Pt loading catalyst for the oxygen reduction reaction in acidic fuel cells, *J. Power Sources* 268 (2014) 171–175.
- [32] A.O. Al-Youbi, J.G. de la Fuente, F. Pérez-Alonso, A.Y. Obaid, J. Fierro, M. Peña, M.A. Salam, S. Rojas, Effects of multiwalled carbon nanotube morphology on the synthesis and electrocatalytic performance of Pt supported by multiwalled carbon nanotubes, *Appl. Catal. B-Environ.* 150 (2014) 21–29.
- [33] C. Galeano, C. Baldizzone, H. Bongard, B. Spliethoff, C. Weidenthaler, J.C. Meier, K.J. Mayrhofer, F. Schüth, Carbon-based yolk-shell materials for fuel cell applications, *Adv. Funct. Mater.* 24 (2014) 220–232.
- [34] C. Galeano, J.C. Meier, M. Soorholtz, H. Bongard, C. Baldizzone, K.J. Mayrhofer, F. Schüth, Nitrogen-doped hollow carbon spheres as a support for platinum-based electrocatalysts, *ACS Catal.* 4 (2014) 3856–3868.
- [35] P. Zhang, Z.-A. Qiao, S. Dai, Recent advances in carbon nanospheres: synthetic routes and applications, *Chem. Commun.* 51 (2015) 9246–9256.
- [36] S. Ikeda, S. Ishino, T. Harada, N. Okamoto, T. Sakata, H. Mori, S. Kuwabata, T. Torimoto, M. Matsumura, Ligand-free platinum nanoparticles encapsulated in a hollow porous carbon shell as a highly active heterogeneous hydrogenation catalyst, *Angew. Chem. Int. Ed.* 118 (2006) 7221–7224.
- [37] G.-H. Wang, J. Hilpert, F.H. Richter, F. Wang, H.-J. Bongard, B. Spliethoff, C. Weidenthaler, F. Schüth, Platinum-cobalt bimetallic nanoparticles in hollow carbon nanospheres for hydrogenolysis of 5-hydroxymethylfurfural, *Nat. Mater.* 13 (2014) 293–300.
- [38] R. Liu, S.M. Mahurin, C. Li, R.R. Unocic, J.C. Idrobo, H. Gao, S.J. Pennycook, S. Dai, Dopamine as a carbon source: the controlled synthesis of hollow carbon spheres and yolk-structured carbon nanocomposites, *Angew. Chem. Int. Ed.* 50 (2011) 6799–6802.
- [39] J. Ying, G. Jiang, Z.P. Cano, L. Han, X.-Y. Yang, Z. Chen, Nitrogen-doped hollow porous carbon polyhedrons embedded with highly dispersed Pt nanoparticles as a

highly efficient and stable hydrogen evolution electrocatalyst, *Nano Energy* 40 (2017) 88–94.

[40] W. Xia, J. Zhu, W. Guo, L. An, D. Xia, R. Zou, Well-defined carbon polyhedrons prepared from nano metal-organic frameworks for oxygen reduction, *J. Mater. Chem. A* 2 (2014) 11606–11613.

[41] R. Banerjee, A. Phan, B. Wang, C. Knobler, H. Furukawa, M. O'keeffe, O.M. Yaghi, High-throughput synthesis of zeolitic imidazolate frameworks and application to CO_2 capture, *Science* 319 (2008) 939–943.

[42] D. He, Y. Jiang, H. Lv, M. Pan, S. Mu, Nitrogen-doped reduced graphene oxide supports for noble metal catalysts with greatly enhanced activity and stability, *Appl. Catal. B-Environ.* 132 (2013) 379–388.

[43] R. Silva, D. Voiry, M. Chhowalla, T. Asefa, Efficient metal-free electrocatalysts for oxygen reduction: polyaniline-derived N-and O-doped mesoporous carbons, *J. Am. Chem. Soc.* 135 (2013) 7823–7826.

[44] C. Song, J. Zhang, Electrocatalytic oxygen reduction reaction, in: J. Zhang (Ed.), *PEM Fuel Cell Electrocatalysts and Catalyst Layers*, Springer, 2008, pp. 89–134.

[45] M. Chiwata, K. Kakinuma, M. Wakisaka, M. Uchida, S. Deki, M. Watanabe, H. Uchida, Oxygen reduction reaction activity and durability of Pt catalysts supported on titanium carbide, *Catalysts* 5 (2015) 966–980.

[46] B. Lim, M. Jiang, P.H. Camargo, E.C. Cho, J. Tao, X. Lu, Y. Zhu, Y. Xia, Pd-Pt bimetallic nanodendrites with high activity for oxygen reduction, *Science* 324 (2009) 1302–1305.

[47] H. Zhang, M. Jin, J. Wang, W. Li, P.H. Camargo, M.J. Kim, D. Yang, Z. Xie, Y. Xia, Synthesis of Pd-Pt bimetallic nanocrystals with a concave structure through a bromide-induced galvanic replacement reaction, *J. Am. Chem. Soc.* 133 (2011) 6078–6089.

[48] S.C. Zignani, E. Antolini, E.R. Gonzalez, Evaluation of the stability and durability of Pt and Pt-Co/C catalysts for polymer electrolyte membrane fuel cells, *J. Power Sources* 182 (2008) 83–90.

[49] L. Dubau, M. Lopez-Haro, L. Castanheira, J. Durst, M. Chatenet, P. Bayle-Guillemaud, L. Guétaz, N. Caqué, E. Rossinot, F. Maillard, Probing the structure, the composition and the ORR Activity of $\text{Pt}_3\text{Co}/\text{C}$ nanocrystallites during a 3422h PEMFC ageing test, *Appl. Catal. B-Environ.* 142 (2013) 801–808.